Optimization of nanopores generated by chemical etching of swift-ion irradiated LiNbO3.

M. Crespillo, M. Otto, A. Muñoz-Martín, J. Olivares, F. Agulló-López, M. Seibt, M. Toulemonde, C. Trautmann

OPTIMIZATION OF NANOPORES OBTAINED BY CHEMICAL ETCHING ON SWIFT-ION IRRADIATED LITHIUM NIOBATE

M. L. Crespillo[a], M. Otto[a,1], A. Munoz-Martin[a], J. Olivares[b,a,*], F. Agulló-López [a,c], M. Seibt[d], M. Toulemonde[e] and C. Trautmann[f].

[a]Centro de Microanálisis de Materiales (CMAM), Universidad Autónoma de Madrid (UAM), Cantoblanco, E-28049 Madrid, Spain.

[b]Instituto de Óptica, CSIC, C/Serrano 121, E-28006 Madrid, Spain.

[c]Departamento de Física de Materiales, Universidad Autónoma de Madrid (UAM) Cantoblanco, 28049 Madrid, Spain.

[d]IV.Physikalisches Institut. Universität Göttingen. Institut für Halbleiterphysik. Tammannstr. 1. D-37077 Göttingen, Germany.

[e]Centre Interdisciplinaire de Recherche Ions-Lasers, UMR 11 CEA-CNRS, 14040 Caen Cedex, France.

[f]Gesellschaft für Schwerionenforschung (GSI), Materialforschung, Planckstrasse 1, 64291 Darmstadt, Germany.

Abstract

The morphology of the nanopores obtained by chemical etching on ion-beam irradiated $LiNbO_3$ has been investigated for a variety of ions (F, Br, Kr, Cu, Pb), energies (up to 2300 MeV), and stopping powers (up to 35 keV/nm) in the electronic energy loss regime. The role of etching time and etching agent on the pore morphology, diameter, depth, and shape has also been studied. The transversal and depth profiles of the pore have been found to be quite sensitive to both irradiation and etching parameters. Moreover, two etching regimes with different morphologies and etching rates have been identified.

*Corresponding author:

José Olivares, Instituto de Óptica, CSIC, C/Serrano 121, E-28006 Madrid, Spain.

E-mail: j.olivares@io.cfmac.csic.es, Tel.: +34 91 497 3670 Fax: +34 914973623

[1]Presently at II. Physikalisches Institut. Universität Göttingen. Friedrich-Hund-Platz 1. D-37077 Göttingen. Germany.

PACS: 81.07.-b; 61.80.Jh; 42.70.Mp.

Keywords: Nanopores, swift ion irradiation, ion tracks, AFM, lithium niobate.

1. Introduction

Nanometer-diameter amorphous tracks are generated by irradiation with swift ions on a variety of dielectric crystals and minerals whenever the electronic stopping power is above a certain threshold value[1-3] (i.e. 5 keV/nm for $LiNbO_3$). These tracks can be chemically etched to produce nanopores and a number of applications[1,4,5] have been tested or suggested including fission-fragment dosimetry, molecular sieves, magnetic storage, field-emission displays,... For most applications the morphology of these nanopores has to be carefully controlled and optimized. So far, latent tracks in $LiNbO_3$ (LN), as relevant photonic material[6], have been produced and characterized by RBS/C and optical methods[7,8]. The kinetics of chemical etching has also been studied by [9-12] SEM and the etching rate measured by profilometry in experiments where the role of nuclear processes is significant[9-12]. On the other hand, very scarce information is available[13] on the detailed morphology of single etched tracks that is the relevant point for nano-patterning applications.

The purpose of this work is to extend and complement previous work[13] to ascertain the role of irradiation conditions (ion energy, ion stopping power) and etching parameters on the morphology of etched tracks. Ions with input stopping powers from 3.4 keV/nm (F at 5 MeV) up to 35 keV/nm (Pb at 2300 MeV) have been used, so that the effects of electronic damage can be easily discriminated from those due to nuclear collisions. The role of thermal annealing after irradiation on the track morphology has been also investigated.

2. Experimental

Congruent $LiNbO_3$ (5x5 mm^2) samples were cut from single crystal optical grade plates purchased from Photox Inc. They were irradiated at normal incidence in the

5 MV tandem accelerator installed at CMAM-UAM, in GANIL (Caen, France) and in GSI (Darmstadt, Germany). The energies, stopping powers (at the surface) and projected ranges of the ions used in this study are listed in Table I. Irradiation fluences were in the 10^7 – 10^9 cm^{-2} fluence range. Chemical etchings were performed at room temperature (RT) in pure HF with concentrations of 5% and 40%, and blends of HF (40%) with HNO3 (70%) in 1:1 ratio. The main characterization technique used for the examination of surface morphology was an AFM commercial instrument from Nanotec Electrónica S.L. with phase-locked loop (PLL) feedback added to the dynamic or tapping mode. Most measurements have been realized using commercial etched single-crystalline silicon nitride tips with a nominal end radius of 10 nm and a resonant frequency of 75 kHz. In certain cases high aspect ratio (>5:1) silicon tips (half cone angle smaller than 5°) and radii of curvature less than 15 nm have been used. The acquisition and analysis was made using the WSxM software, which is distributed freely by Nanotec Electrónica S.L. AFM investigations were performed on X-cut samples to avoid the strong tip-surface interaction typically observed through the experience for Z-cut samples (piezoelectric behavior of $LiNbO_3$). For further structural characterization of the nanopores the Philips CM200-FEG-UT transmission electron microscope (TEM) was used. Samples were prepared with the focused ion beam (FIB) and a gold film of 200 nm thickness was vapour deposited on the surface. All images were recorded in bright field mode.

3. Results

3.1. *TEM data*

The TEM morphology of latent tracks generated on a $LiNbO_3$ sample (Z-cut) by irradiation with Cu^{9+} ions at 51 MeV is illustrated in Fig. 1a captured with 40 kV.

111 The contrast is high enough to reveal the latent tracks. The tracks show a diameter value
112 of around 9 nm at the surface. For comparison the image of a crack of 18 nm diameter
113 and 305 nm depth is shown. The insets A and B in the figure correspond to the
114 diffraction patterns obtained on the crystalline region and inside the track respectively,
115 and they were recorded from a high resolution transmission electron microscope
116 (HRTEM) measurement with an acceleration voltage of 300 kV, similar to the one used
117 for the image shown in Fig. 1b. One notices the marked disorder apparent in the inset B.
118 In inset A, much more reflections are present than in B, which indicates that the crystal
119 structure changed and some kind of a phase transition has taken place. However we
120 have to take in account that since these HRTEM measurements are cross sections some
121 signal may come from the crystalline material surrounding the track. Further
122 investigations taking plan view measurements (i.e. along the track) must be carried out.
123 Fig. 1.b shows after etching time a very broad surface "crater" of 34 nm
124 diameter and 3.5 nm depth, whose symmetry axis is clearly shifted in relation to that for
125 the non-etched track.
126
127 3.2. *Effect of irradiation on nanopore morphology*
128 The track morphology after etching markedly depends on the irradiation conditions:
129 ion and energy. Some of the AFM pictures are shown in Fig. 2a, b, c and d,
130 corresponding to ions and energies indicated on the images. For stopping powers close
131 to the threshold value (5 keV/nm), as for F at 5 MeV (a), the shape of the nanopores
132 exhibits axial symmetry and is approximately circular. The same shape is also observed
133 for larger stopping powers at low enough etching times (≤ 10 min) and weaker acid
134 concentration (HF 5% and blends). On increasing stopping power and standard etching
135 times (20-60 minutes at RT) the pores clearly develop a pyramidal structure with well-

136 defined facets, as illustrated by the irradiations with Br at 46 MeV (Fig. 2b). At even
137 higher stopping powers, i.e. for irradiations with Kr at 800 MeV (Fig. 2c) and Pb at
138 2300 MeV (Fig. 2d), the faceting turns into a rather smooth and elongated profile. The
139 long axis lies at 33° from the z crystallographic axis (see Fig. 5.a) and so approximately
140 coincides with the easy cleavage plane[6]. Track etch pit has a double-shape well that was
141 also observed in our previous work[13]. It has been checked that the above morphological
142 trend is independent of the AFM tip used for the observations and the scanning
143 direction.

144 In order to better understand the origin of the pore asymmetry, we have investigated
145 the effect of Br irradiation at 46 MeV on +X and -X faces on the pore morphology. The
146 results are displayed in Fig. 3 that shows a chiral behavior i.e. the two pore images are
147 mirror images to each other.

148

149 3.3. *Effect of etching time in acid aqueous solutions.*

150 The evolution of the pore diameter and pore depth with etching time at RT is
151 respectively illustrated in Fig.4a and 4b for the irradiation with Br at 46 MeV. Data for
152 three acid solutions are included: HF at 40 %, HF at 5% and 1:1 mixture of both acids
153 (HF 40%, HNO_3 70%). The most efficient etching is with HF at 40%. The etching rate
154 is much larger than that obtained in a previous study with a 1:1 mixture of HF and
155 HNO_3. The aspect ratio defined as depth/diameter is plotted in Fig. 4c.

156

157 3.4. *Influence of thermal annealing*

158 Thermal treatments after irradiation may anneal out some of the defects generated in
159 and around the track and thus influence the subsequent etching rates and pore
160 morphologies. The results are illustrated in Fig. 5 corresponding to the irradiation with

Br ions of 46 MeV, followed by, annealing in air for 60 minutes at various temperatures as marked on the AFM images, and finally etched in HF 40%, for 60 minutes. One observes that the annealing treatment does not remove entirely the latent tracks. Moreover, it induces a clear elongation of the pore shape and gives rise to higher surface aspect ratios.

4. Conclussion

Our extended set of etching experiments confirms that the pore morphology strongly depends on the concentration of the acid solution and etching time. Pores initially exhibit approximately axial symmetry but under extended etching they develop well defined facets that correspond to particular crystalline planes. The faceted morphology, not previously observed for $LiNbO_3$, has also been observed in other crystals[14]. Since $LiNbO_3$ is non centro symmetric, the morphology on the +X and –X faces of the sample are mirror images from one another. Finally, many facets develop and the shape rounds up but showing a very clear elongated anisotropy. The extrapolation of the data in Fig. 4 to $t = 0$ indicate that the initial etching rate is quite fast up to about a (circular) pore diameter of 10-40 nm and a depth of a few nanometers depending on the stopping power of the ion. This fast stage could be associated to the track core (with a diameter of a few nanometers) including the highly defective surrounding halo whose diameter amounts to about 2-3 times that of the core[15]. The initial radial etch rate stage is followed by a linear slower stage (where facets develop) that reaches an average diameter of a few hundred of nanometers and a depth close to 100 nm. The slow stage has a rate of a few nm/min depending on the concentration and composition of the acid solution and should correspond to the etching of crystalline $LiNbO_3$, i.e. the etching rate should be essentially equal to that of the bulk unirradiated material.

Acknowledgements:

We acknowledge funding from the project MAT2005-06359-C03-02 from Ministry of Education and Science of Spain. Authors acknowledge to the technical staff of CMAM-UAM.

References

[1] R. Spohr, in. K. Bethge (Ed.), *Ion tracks and Microtechnology, Basic Principles and Applications,* Vieweg, 1990.

[2] G. Szenes, Phys. Rev. **B 51**, 8026 (1995).

[3] A. Meftah, J.M. Costantini, N. Khalfaoui, S. Boudjadar, J.P. Stoquert, F. Studer and M. Toulemonde, Nucl. Instrum. Meth. Phys. Res. **B 237**, 563 (2005).

[4] M. Toulemonde, C. Trautmann, E. Balanzat, K. Hjort and A. Weidinger, Nucl. Instrum. Meth. Phys. Res. **B 216**, 1 (2004).

[5] J-H. Zollondz, and A. Weidinger, Nucl. Instrum. Meth. Phys. Res. **B 225**, 178 (2004).

[6] R. S. Weis and T.K. Gaylord, *Applied Physics A: Materials Science and Processing,* **37,** 191 (2004).

[7] S.M.M. Canut, R. Ramos, P. Brenier, J.L. Thevenard and M. Toulemonde, Nucl.Instrum. Meth. Phys. Res. **B 107**, 194 (1996).

[8] J. Olivares, A. García-Navarro, G. García, A. Méndez and F. Agulló-López, Appl. Phys. Lett. **89**, 1 (2006).

[9] M. Levy, R.M. Osgood Jr., R. Liu, E. Gross, G.S. Cargill III, A. Kumar, H. Bakhru, Appl. Phys. Lett. **73**, 2293 (1998).

[10] C.L. Sones, S. Mailis, W.S. Brocklesby, R.W. Eason and J.R. Owen, J. Mater. Chem. **12**, 295 (2002).

[11] J. Reinisch, F. Schrempel, T. Gischkat and W. Wesch, J. Electrochem.Soc. **155 (4),** D298 (2008).

[12] M. Bianconi, F. Bergamini, G.G. Bentini, A. Cerutti, M. Chiarini, P. De Nicola, G. Pennestri, Nucl. Instrum. Meth. Phys. Res. (2008) (in press).

[13] A. García-Navarro, A. Méndez, J. Olivares, G. García, F. Agulló-López, M. Zayat, D. Levy and L. Vazquez, Nucl. Instrum. Meth. Phys. Res. **B 249**, 172 (2006).

[14] C. Trautmann, K. Schwartz, J. M. Costantini, T. Steckenreiter and M. Toulemonde, Nucl. Instrum. Meth. Phys. Res. **107 B**, 367 (1998).

[15] J. Olivares, A. García-Navarro, G. García, A. Méndez and F. Agulló-López, Appl. Phys. Lett. **89**, 071923 (2006).

6. Table list.

Table 1

Ion	Energy [MeV]	Energy [MeV/amu]	Se [keV/nm]	Rp [μm]
F	5	0.26	3.4	2.5
Br	12	0.15	6.1	3.2
Br	22	0.29	8.8	4.5
Br	46	0.57	12	6.7
Cu	51	0.80	12	7.2
Kr	800	10.4	13	60
Pb	2300	11.1	35	78

Table captions:

Table I: Energies, electronic stopping powers at the surface, (Se) and projected ranges (Rp) of the ions used.

7. Figure captions.

Fig. 1. TEM images of Cu 51 MeV irradiated $LiNbO_3$. (a) The light stripes indicate the unetched tracks induced by ion bombardment; insets show the diffraction patterns; (b) HRTEM image showing etched nanopore in cross sectional view.

Fig. 2. AFM images of different etch pit morphologies obtained after etching tracks (HF 40% at RT for different times) produced with different kind of ions and energies: (a) F 5 MeV, after 60 min., (b) Br 46 MeV, after 60 min., (c) Kr 800 MeV, after 10 min. and (d) Pb 2300 MeV, after 10 min. Different AFM image sizes and depth-scales have been used. The inset in (d) shows the depth profile recorded along the line across the long axis of the two elongated pores. The lines are the polishing scratches revealed after etching process in (a).

Fig. 3. AFM images of etched tracks on the + *X* face (a) vs. the –*X* face (b) of lithium niobate after irradiation with Br 46 MeV and etched during 60 min in HF 40% at RT. Revealed facets appear clearly in the excitation frequency image recorded by PLL mode shown as inset in each case. Depth-scale: 30 nm.

Fig. 4. Pore dimensions versus etching time for different etching solutions using samples irradiated with Br ions of 46 MeV. (a) Long axis diameter, (b) pore depth, and (c) aspect ratio (depth/ short axis diameter).

Fig. 5. AFM images of pore morphologies obtained for samples irradiated with Br ions of 46 MeV and subjected to annealing in air for 1 hour at different temperatures, prior to the etching process (HF 40%, 1 hour at RT). Depth-scale: 30 nm.

8. Figures

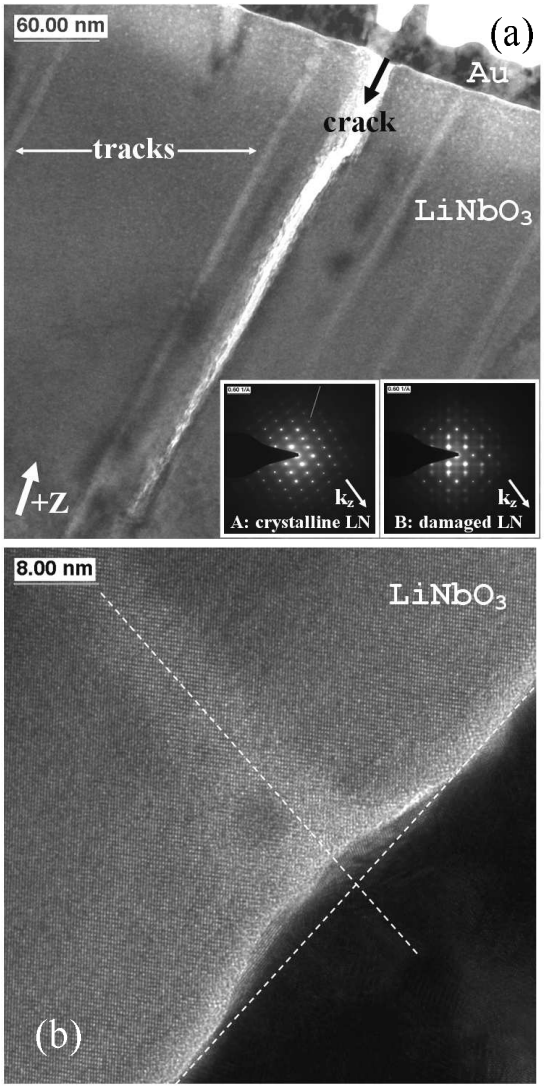

Fig. 1

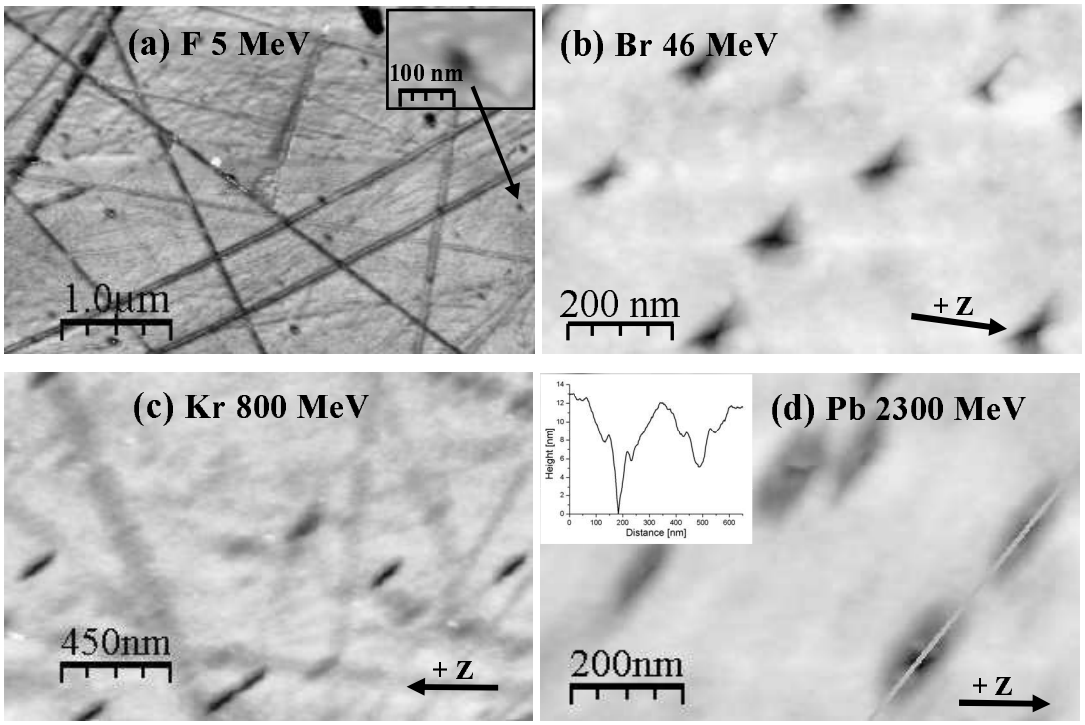
(a) F 5 MeV
100 nm
1.0μm
(b) Br 46 MeV
200 nm
+z
(c) Kr 800 MeV
450nm
+z
Height [nm]
Distance [nm]
(d) Pb 2300 MeV
200nm
+z

Fig. 2

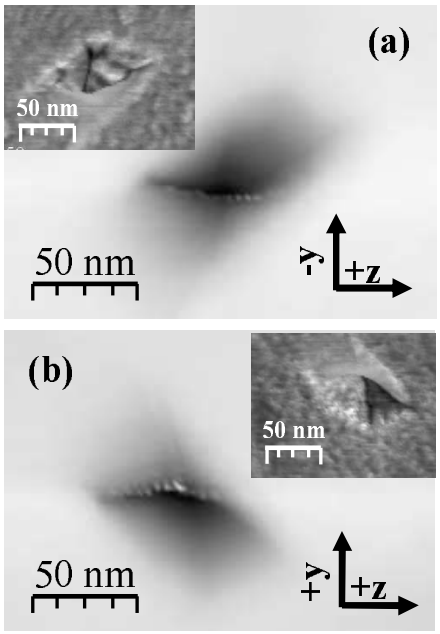

Fig. 3

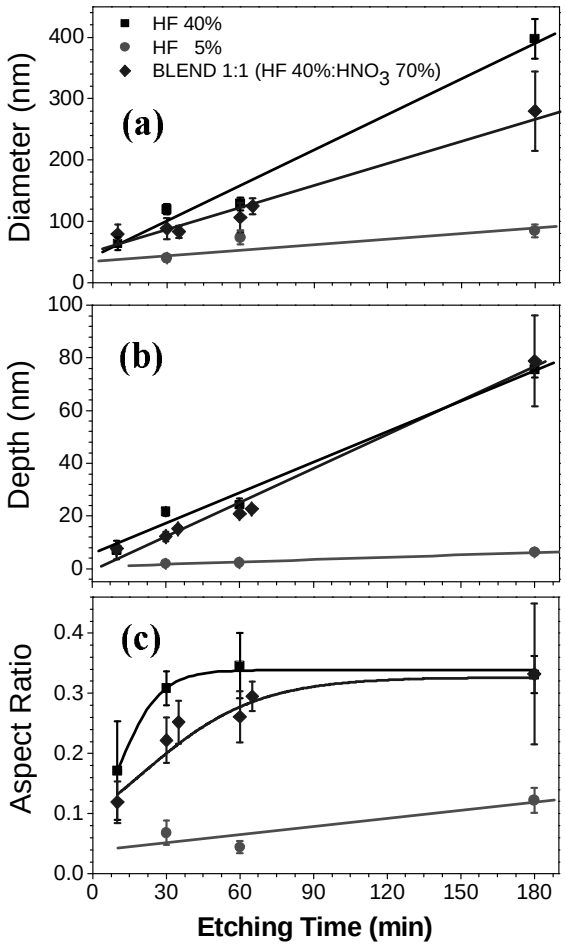
HF 40%
HF 5%
BLEND 1:1 (HF 40%:HNO3 70%)
(a)
Diameter (nm)
(b)
Depth (nm)
(c)
Aspect Ratio
Etching Time (min)

Fig. 4

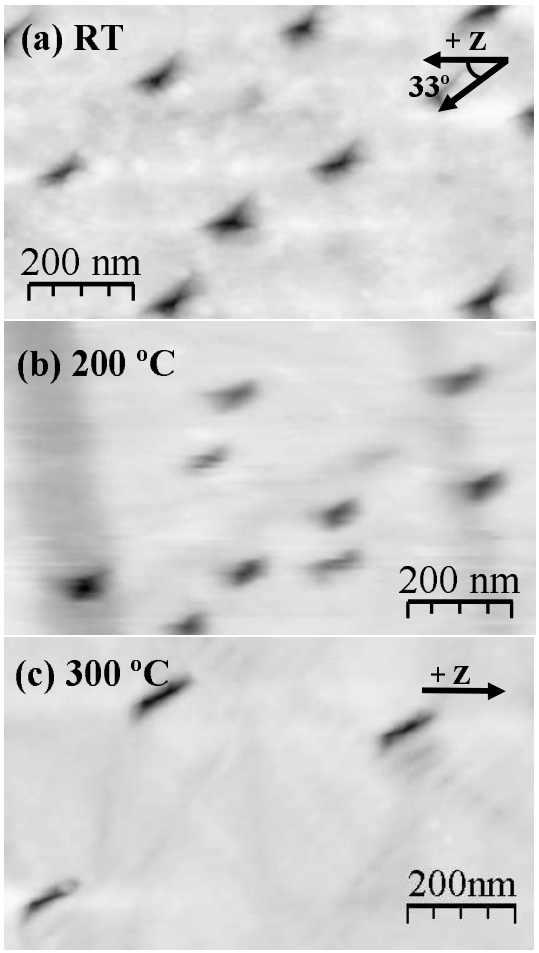

Fig. 5